

# An Investigation of FP8 Across Accelerators for LLM Inference

Jiwoo Kim <sup>\*1</sup> Joonhyung Lee <sup>\*2</sup> Gunho Park <sup>2</sup> Byeongwook Kim <sup>2</sup> Se Jung Kwon <sup>2</sup> Dongsoo Lee <sup>2</sup>  
Youngjoo Lee <sup>1</sup>

## Abstract

The introduction of 8-bit floating-point (FP8) computation units in modern AI accelerators has generated significant interest in FP8-based large language model (LLM) inference. Unlike 16-bit floating-point formats, FP8 in deep learning requires a shared scaling factor. Additionally, while E4M3 and E5M2 are well-defined at the individual value level, their scaling and accumulation methods remain unspecified and vary across hardware and software implementations. As a result, FP8 behaves more like a quantization format than a standard numeric representation. In this work, we provide the first comprehensive analysis of FP8 computation and acceleration on two AI accelerators: the NVIDIA H100 and Intel Gaudi 2. Our findings highlight that the Gaudi 2, by leveraging FP8, achieves higher throughput-to-power efficiency during LLM inference, offering valuable insights into the practical implications of FP8 adoption for datacenter-scale LLM serving.

## 1. Introduction

The FP8 format has emerged as a promising datatype due to its lower computational overhead, reduced power consumption, and improved memory efficiency compared to commonly used formats such as FP32 and BF16 (Kalamkar et al., 2019), particularly at large batch sizes. With the introduction of the Intel Gaudi HPU and NVIDIA Hopper GPUs, FP8 is gaining traction as a key datatype for next-generation AI workloads (DeepSeek-AI, 2024).

While extreme low-bit quantization has been widely studied, its throughput remains inferior to conventional 16-bit floating-point formats on commercial hardware (Lin et al., 2024b). In contrast, FP8 has rapidly become the preferred format due to its compatibility with existing accelerators while preserving model accuracy. This makes it particularly

<sup>\*</sup>Equal contribution <sup>1</sup>Department of Electrical Engineering, Pohang University of Science and Technology, Pohang, Republic of Korea <sup>2</sup>NAVER Cloud, Seongnam, Republic of Korea.

well-suited for datacenter-scale LLM inference, where both high throughput and minimal accuracy degradation are critical. In some accelerators, FP8 can be twice as fast as BF16. Given the immense computational costs of training and deploying large language models (LLMs), FP8 has garnered significant attention for its potential efficiency gains.

Despite its advantages, FP8 utilization is constrained by the widening gap between computing speed and memory bandwidth. A key challenge is that, while LLM sizes continue to scale, their hidden dimensions grow at a much slower rate (e.g., Llama 8B has a hidden size of 4096, but Llama v3.70B only increases hidden size to 8192). Tensor parallelism (TP) further partitions matrices into even smaller fragments, making small matrix efficiency a critical performance factor.

Especially during the decode phase, Generalized Matrix-Vector (GEMV) and thin General Matrix-Matrix Multiply (GEMM) operations dominate, reducing Model FLOP Utilization (MFU) (Chowdhery et al., 2023; Narayanan et al., 2021). With the growing popularity of “reasoning” models (DeepSeek-AI, 2025), the proportion of decoding in LLM inference workloads can be expected to continue growing.

To comprehensively address the challenges of LLM inference, we aim to quantify the various constraints that impact performance, including those introduced by FP8 quantization. To the best of our knowledge, we are the first to provide quantitative measurements associated with various FP8 quantization schemes.

There is a notable lack of research providing comprehensive FP8 experimental results, particularly in studies analyzing hardware characteristics in LLM inference configurations. To address this gap, our work offers a detailed evaluation of FP8 performance across different hardware platforms, providing valuable insights for model developers on the trade-offs between model architecture and hardware design. To summarize our contributions:

1. We analyze scaling factor configurations for FP8 formats and quantify key LLM inference constraints in datacenter environments, providing a unified framework to compare throughputs across different inference stages, model sizes, and sequence lengths.
2. We analyze the computational characteristics of LLM

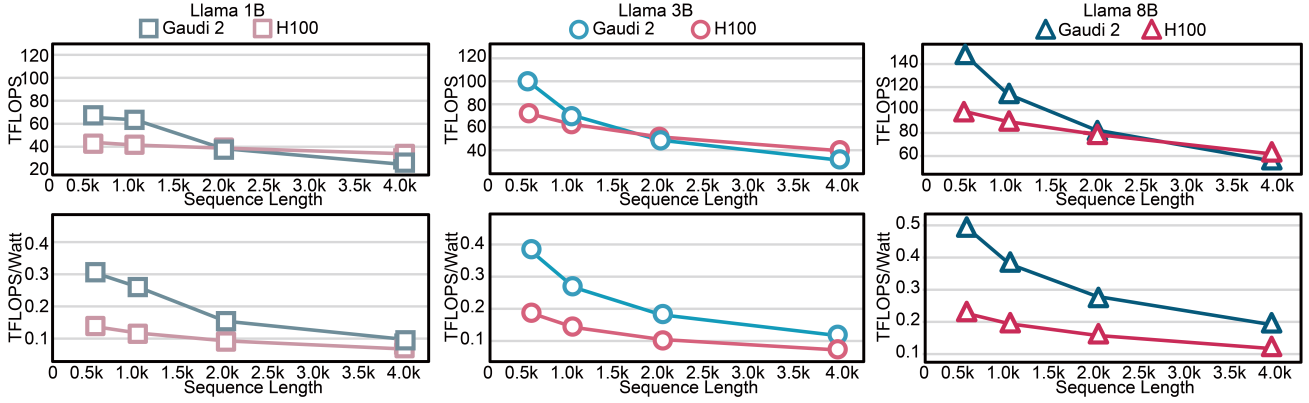


Figure 1. TFLOPS (top row) and TFLOPS/Watt (bottom row) comparison between the Gaudi 2 and H100 using FP8 in the decode phase with batch size set to 64. We measure inference throughput using Optimum Habana v1.15.0 for the Gaudi 2 and TensorRT-LLM v0.16.0 for the H100. For short sequences, the Gaudi 2 has an advantage both in absolute throughput and in TFLOPS/Watt. At longer sequences, the H100 achieves higher TFLOPS due to its superior memory bandwidth, but is less energy efficient due to higher power consumption.

inference on the Gaudi 2 and H100 across both the prefill and decode phases. In the prefill phase, where compute performance is the key factor, H100’s throughput is 50% higher than Gaudi 2’s. However, since the decode phase dominates overall inference time, accelerator utilization becomes more critical, and Gaudi 2 achieves 50% higher throughput in this phase. This highlights the differing performance trade-offs between the two accelerators across LLM inference workloads.

## 2. Background

With the explosive growth of LLM sizes in recent years, numerous techniques specific to generative LLMs have emerged to reduce memory requirements and improve output speeds. In this work, we focus on the large-batch serving environment often found in data centers, where multiple requests for LLM inference run simultaneously under power constraints at both the rack and data center levels.

Various methods have been proposed to improve LLM serving efficiency, with quantization being one of the most widely studied. However, a key challenge in LLM quantization is the presence of activation outliers. Transformer models often contain large outlier values in their activations, which, if not properly addressed during quantization, can lead to substantial quality degradation (Sun et al., 2024a). To mitigate this issue, several quantization techniques have been developed, aiming to improve robustness and accuracy while maintaining computational efficiency.

### 2.1. Weight-only quantization

Due to the quantization difficulties posed by activation outliers, many studies have proposed several weight-only quantization (WoQ) methods (Lin et al., 2024a; Frantar et al., 2023; Lee et al., 2023), while retaining activations in BF16

or FP16 format. However, these approaches often suffer from low throughput at larger batch sizes. To enable computations, quantized weights must be converted into the same data type as activations (e.g. BF16), requiring online dequantization. This is handled by CUDA cores on NVIDIA GPUs and TPC cores on Gaudi HPUs, which operate an order of magnitude slower than their respective matrix multiplication units. Therefore, dequantization frequently becomes a bottleneck even at moderate batch sizes. Also, because GEMM computations are conducted at higher precisions, WoQ methods are fundamentally limited to having the same throughput as unquantized GEMMs at best.

Even when high throughput is achieved, kernel implementations often need to be re-implemented for different devices, including those from the same vendor. For instance, the Marlin kernel (Frantar et al., 2024), optimized for int4-weight and float16-activations on the A100, is suboptimal for the H100. As a result, the Machete kernel (Wilkinson, 2024) was developed specifically to leverage the new features of the Hopper architecture, employing different design trade-offs. These challenges arise due to variations in cache sizes, hardware features, and compute-to-memory bandwidth ratios, all of which necessitate different optimizations to achieve high performance. Consequently, adapting WoQ methods across different accelerators imposes significant implementation overhead and increases development costs.

### 2.2. INT8 quantization

The INT8 quantization format described in Xiao et al. (2024) is closely related to our work, requiring quantization of both weights and activations to leverage INT8 tensor cores to accelerate computations. While INT8 quantization has been widely adopted in fields such as computer vision, its limited dynamic range presents challenges in achieving full accuracy for LLM inference. FP8 thus has an advantage

over INT8 as integer representations are inherently less robust to outliers compared to floating-point numbers (Shen et al., 2024; Kurtic et al., 2024).

### 2.3. FP8 quantization

The FP8 format can be categorized into two variants based on the allocation of bits to the exponent and mantissa: the E4M3 format and the E5M2 format. E4M3 offers higher precision compared to the E5M2 format, which instead has a higher dynamic range. To address the smaller dynamic range of FP8 compared to BF16, scaling factors are employed to adjust the inputs before casting to FP8. This ensures that the values fit within the FP8 range, maximizing the utilization of its limited dynamic range. Per-tensor scaling, which computes a single scaling factor for each matrix. For more granular control, per-token scaling can be applied to activations, while per-channel scaling is used for weights, enabling finer adjustments. Group-wise scaling factors (DeepSeek-AI, 2024) have also been proposed.

### 2.4. Scaling factor computation

A critical consideration for activation quantization is the overhead of converting activations to lower precision. While non-linear operations require 16-bit or even 32-bit precision, activations must be quantized online immediately before GEMM computations utilize low-precision compute units. This introduces non-trivial overhead, limiting the throughput gains from reduced precision. Activation quantization also requires estimating input statistics to determine appropriate scaling factors. A direct approach, measuring statistics for each activation before quantization, would necessitate two memory accesses: one for collecting statistics and another for quantization, incurring high latency. To mitigate this, many libraries use a calibration set to precompute scaling factors based on a representative sample of activations.

A key limitation of static scaling is that it typically enforces per-tensor scaling of activations, as token-wise variations are unknown in advance. For instance, altering the order of sequences during batched decoding would shift token positions. Moreover, using position-dependent scaling factors would require fixed input sizes. While per-channel scaling (Xiao et al., 2024) is possible, the same scaling factors are still applied to all tokens, potentially reducing accuracy.

In contrast, dynamic scaling is more efficient when applied separately to each token as measurement and quantization can be combined in a single memory access. It also enables group-wise quantization, as implemented in DeepSeek-AI (2024) with a group size of 128, improving output quality through finer-grained scaling factors.

A potential optimization for both scaling methods is to merge quantization with other memory-bound operations. In

Pre-LN Transformers (Xiong et al., 2020), activation quantization can be fused with RMSNorm. Similarly, element-wise multiplication in SwiGLU (Shazeer, 2020) can also be fused. Frameworks such as TensorRT-LLM (NVIDIA, 2023) v0.16.0 have already implemented these optimizations for FP8 activation quantization. They have yet to be implemented for Gaudi HPUs as of the time of writing.

### 2.5. LLM evaluation

LLM evaluation has grown in importance as new LLMs compete for prominence. Traditionally, WikiText-2 perplexity (Merity et al., 2017) has been widely used due to its ease of measurement and relationship with the training loss. More recently, Massive Multitask Language Understanding (MMLU) (Hendrycks et al., 2021) has emerged as the *de facto* standard to assess LLM quality, evaluating knowledge in a wide range of domains. However, multiple-choice benchmarks may fail to capture the full impact of quantization. For instance, the Llama v3 405B model (Llama Team, 2024) applies max-absolute (maxabs) clipping when calculating scaling factors despite there being no effect in standard evaluation metrics because the model may generate corrupted outputs for high-perplexity tokens, such as dates, without maxabs clipping.

Moreover, evaluation should extend beyond pre-trained base models to instruction-tuned models that have undergone alignment. If quantization is applied after pre-training but before alignment, the alignment process must be quantization-aware, requiring each quantization algorithm to be integrated with each alignment method while maintaining alignment quality, significantly increasing complexity. For this reason, we conduct all evaluations on instruction-tuned models, where quantization effects are more representative of real-world deployment scenarios.

## 3. Matrix multiplication comparison

### 3.1. Differences in hardware capabilities

We compare implementations of FP8 GEMM between NVIDIA GPUs and Intel Gaudi HPUs, identifying key differences despite both adhering to the FP8 specification (Mikikevicius et al., 2022).

**(Accumulation precision)** Hopper GPUs use a 14-bit accumulator for FP8 GEMMs (DeepSeek-AI, 2024), requiring casting to CUDA cores for higher precision. Software optimizations, such as applying FP32 accumulation to only one in four WGMMA instructions, reduce error but increase kernel complexity and remain less precise than full FP32 accumulation. In contrast, Gaudi HPUs always accumulate in FP32, ensuring higher numerical precision.

**(E4M3 range)** The Gaudi 2 follows the IEEE specification

for special values, unlike NVIDIA GPUs, which use a single special value representation (Noune et al., 2022). This results in seven fewer magnitude representations and a maximum value of 240 for E4M3 in the Gaudi 2 compared to 448 on NVIDIA GPUs. This has been addressed in the Gaudi 3, but we were unable to test these in our experiments.

**(Power-of-2 scaling)** Gaudi HPUs allow modification of floating-point exponent biases to accelerate scaling factor application. The Gaudi 2 supports fixed hardware-accelerated scaling factors of  $2^{-8}, 2^{-4}, 2^0, 2^4$  for E4M3 while the Gaudi 3 extends this to arbitrary powers of 2 between  $2^{-32}$  and  $2^{31}$ . However, this feature is limited to GEMMs with per-tensor scaling factors.

**(Stochastic rounding)** During FP8 quantization, stochastic rounding can be applied when converting 16/32-bit floating-point values to FP8, similar to the technique proposed for FP32-to-BF16 conversion in (Fan et al., 2024). This method is distinct from stochastic rounding applied at the inner-product (El Arar et al., 2023).

**(Sparsity)** NVIDIA GPUs support semi-structured sparsity acceleration, potentially doubling tensor core peak throughput. However, despite attempts to leverage sparsity in LLMs (Frantar & Alistarh, 2023; Sun et al., 2024b), dense GEMMs remain dominant due to accuracy loss and limited speedups. Gaudi HPUs do not support sparsity acceleration.

### 3.2. GEMM throughput measurements

For a GEMM between matrices of size  $(M \times K) \times (K \times N)$ , the total number of floating-point operations (FLOPs) performed is  $2MKN$ . This is derived from the  $M \times N$  dot products of length  $K$ , where each element undergoes one multiplication and one addition. Following the convention where FLOPS denotes FLOPs per second, we compute throughput in FLOPS using the theoretical FLOPs and the measured latency. We can thus calculate the MFU by dividing observed throughput by peak throughput.

As LLM computations are dominated by matrix multiplications, GEMM throughput serves as an upper bound for model end-to-end performance. While accelerator specifications list peak throughput values, actual throughput rarely reaches this limit, particularly for small matrices.

Table 1 presents GEMM throughput and power consumption measurements for row-wise scaled FP8 GEMM. We conducted measurements on NVIDIA H100 GPUs using the NGC PyTorch 24.12 image and on Intel Gaudi 2 HPUs using the Synapse AI v1.19.0 image. Power consumption was recorded via the "nvidia-smi" and "hl-smi" utilities, respectively. Input casting overheads were excluded from the measurements. Additional results for GEMM throughputs under different conditions are provided in Tables 8 and 9. Our results show that the Gaudi 2 achieves higher utilization

*Table 1.* Throughput and power measurements for square FP8 GEMMs with row-wise scaling. The ratio of measured TFLOPS and power draw relative to their peak values are included in parentheses. We include the TFLOPS/Watt ratio on the right. H100 has 1989.9 peak FP8 GEMM TFLOPS and 700W TDP. Gaudi 2 has 865 peak FP8 GEMM TFLOPS and 600W TDP.

Device	(M,K,N)	TFLOPS	Power (W)	TF/W
Gaudi 2	1K	367.9 (42.5%)	375 (63%)	1.0
	2K	586.2 (67.8%)	460 (77%)	1.3
	4K	817.1 (94.5%)	460 (77%)	1.8
	8K	741.8 (85.8%)	490 (82%)	1.5
H100	1K	218.3 (11.0%)	350 (50%)	0.6
	2K	879.7 (44.2%)	690 (99%)	1.3
	4K	1167.6 (58.7%)	690 (99%)	1.7
	8K	1084.7 (54.5%)	690 (99%)	1.6

than the H100, particularly for small matrices. The performance drop for smaller matrices is steeper on the H100, with the Gaudi 2 providing a higher TFLOPS at matrix sizes of 1K. Also, the Gaudi 2 exhibits lower power consumption than its stated 600W TDP, whereas the H100 approaches its peak 700W TDP even at moderate utilizations.

Unlike NVIDIA GPUs, which incorporate multiple small matrix multiplication accelerators, Gaudi HPUs feature a few large matrix accelerators. As a result, Gaudi HPUs require fewer input elements per cycle to fully utilize compute resources, thereby reducing first-level memory bandwidth requirements and improving efficiency (Intel, 2022; 2024). Additionally, Gaudi HPUs leverage a graph compiler to dynamically reconfigure the MME size based on the target GEMM dimensions, optimizing resource utilization.

This superior efficiency of the Gaudi 2 for small matrices is particularly relevant given that LLM hidden dimensions typically range between 1K (e.g., Llama 1B) and 8K (e.g., Llama 70B), with tensor parallelism further reducing matrix sizes. Moreover, the lower power draw of the Gaudi 2 relative to its TDP suggests that naïve TDP comparisons can be misleading, emphasizing the need for empirical evaluation.

## 4. Comparing end-to-end results

We conduct evaluations on different FP8 features and come to the following conclusions. First, E4M3 consistently outperforms E5M2 in quantization accuracy across nearly all tested configurations. Second, stochastic rounding during quantization has minimal impact on model accuracy and, in some cases, may even be detrimental. Third, dynamic scaling achieves accuracy comparable to BF16 models while eliminating the need for a calibration set.

For evaluation, we use instruction-tuned versions of Llama v3.2 1B, v3.2 3B, v3.1 8B, and v3.3 70B. Unless stated

Table 2. The “Cited” columns include results from Kim (2025) using static “FP8 (S)” scaling from the Intel Neural Compressor (INC) library using the UltraChat 200K (Ding et al., 2023) dataset for calibration. The “Measured” column includes results for dynamic “FP8 (D)” scaling. Reference BF16 accuracies are included for both columns to control for evaluation condition differences.

Llama v3.1 8B Inst.	Cited		Measured	
	BF16	FP8 (S)	BF16	FP8 (D)
MMLU CoT 5-shot	68.4%	66.3%	68.8%	68.3%
GSM8K CoT 5-shot	75.7%	70.4%	83.1%	84.5%
Winogrande	78.1%	77.6%	73.8%	73.8%
TruthfulQA mc1	37.1%	34.9%	39.9%	39.4%
TruthfulQA mc2	54.0%	52.2%	55.1%	54.3%

otherwise, models employ dynamic row-wise scaling for all linear layers, while LM head remains in BF16.

#### 4.1. Dynamic vs static scaling

Section 2 describes the trade-offs between static and dynamic scaling for activation quantization. Static scaling offers higher throughput for large matrices as scaling factors do not need to be computed for each input. It also enables per-tensor quantization, leading to improved GEMM utilization. In contrast, dynamic scaling enhances output quality by assigning separate scaling factors to each token.

Table 2 presents a comparative analysis of model output quality on static vs. dynamic FP8 scaling. The results indicate that dynamic quantization obtains results similar to the original BF16 models, whereas static quantization leads to noticeable accuracy degradation. While various techniques, such as those proposed by Xiao et al. (2024); Liu et al. (2024); Ashkboos et al. (2024), can potentially mitigate this degradation, they still pose a risk as the scaling factors obtained during calibration may be suboptimal for unseen inputs. Therefore, dynamic quantization is the preferred approach, provided that the associated throughput reduction remains within acceptable limits.

#### 4.2. E4M3 vs. E5M2

Following on the findings of Shen et al. (2024), which demonstrated that the E4M3 format achieves superior accuracy on language tasks compared to E5M2, we extend this analysis to instruction-tuned models in Table 3.

To determine the optimal format for inference, we conducted a comparative evaluation of E4M3 and E5M2, measuring MMLU accuracy using LM Evaluation Harness (v0.4.7, (Gao et al., 2024)). Our experimental results consistently indicate that E4M3 outperforms E5M2 across all evaluated scenarios. Furthermore, as shown in Table 8, the GEMM throughputs using E4M3 and E5M2 are comparable, making

Table 3. Comparison between different FP8 data types and rounding modes for MMLU CoT 5-shot performance on instruction-tuned Llama models. Stochastic rounding provides little or no benefit to accuracy while E5M2 is detrimental, especially for smaller models. Experiments were conducted on a Gaudi 2 HPU.

Model	Data Type	Rounding	MMLU
Llama v3.2 1B Instruct	BF16	-	46.3%
	E4M3	SR	45.7%
	E4M3	RTN	45.5%
	E5M2	RTN	44.5%
Llama v3.2 3B Instruct	BF16	-	61.8%
	E4M3	SR	61.7%
	E4M3	RTN	61.6%
	E5M2	RTN	60.7%
Llama v3.1 8B Instruct	BF16	-	68.8%
	E4M3	SR	68.3%
	E4M3	RTN	68.3%
	E5M2	RTN	67.5%
Llama v3.3 70B Instruct	BF16	-	82.0%
	E4M3	SR	82.0%
	E4M3	RTN	82.0%
	E5M2	RTN	82.2%

E4M3 the preferred choice for inference even considering the smaller representational capacity of E4M3 on Gaudi 2.

#### 4.3. Stochastic rounding

Hardware-accelerated stochastic rounding during FP8 quantization is a distinctive feature of Gaudi HPUs, similar to the approach proposed by Fan et al. (2024), and is unavailable in NVIDIA GPUs. Equation 1 formalizes the concept, where a higher-precision value  $x$  is rounded up to  $x_{up}$  or down to  $x_{down}$  stochastically based on the distance from  $x$ .

$$x_{quantized} = \begin{cases} x_{up} & (p = \frac{x - x_{down}}{x_{up} - x_{down}}) \\ x_{down} & (p = \frac{x_{up} - x}{x_{up} - x_{down}}) \end{cases} \quad (1)$$

Stochastic rounding is expected to preserve more of the original numerical information post-quantization, potentially leading to improved model accuracy. However, empirical results in Table 3 indicate that stochastic rounding during quantization does not significantly enhance model accuracy. Furthermore, as shown in Table 6, it may even lead to accuracy degradation in certain cases. These findings suggest that while stochastic rounding during quantization theoretically retains more information, its practical benefits for FP8 inference in LLMs remains inconclusive.

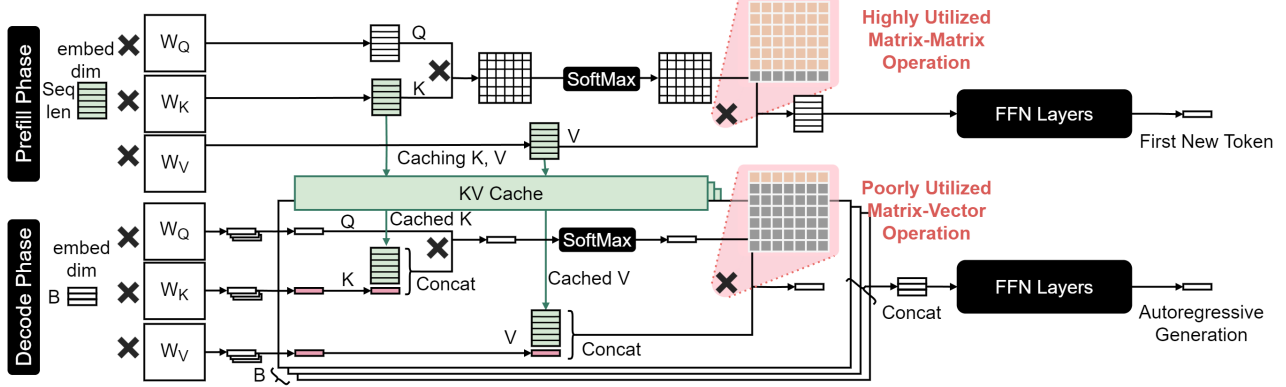


Figure 2. Process and utilization characterization of the two phases of generative LLM inference.

## 5. LLM inference comparison

### 5.1. LLM inference phases

Generative LLM inference comprises two distinct phases: a compute-bound prefill phase and a memory-bound decode phase (Patel et al., 2024; Zhong et al., 2024). Figure 2 illustrates the key differences between these phases.

During the prefill phase, the LLM generates the first token based on the provided input prompt. Throughout this process, key-value (KV) pairs are stored in the KV cache for reuse in subsequent token generations. The prefill phase processes the entire input in parallel, utilizing matrix-matrix operations that are typically compute-bound. This high degree of parallelism allows for effective hardware utilization, enabling efficient input processing.

Once the first token is generated, the process transitions to the decode phase, where output tokens are generated sequentially in an autoregressive manner based on the previous tokens. Unlike the prefill phase, the decode phase is constrained by memory bandwidth, as it involves GEMV operations, which inherently limit hardware utilization compared to the more parallelizable GEMMs in the prefill phase.

Modern inference frameworks such as vLLM (Kwon et al., 2023) and TensorRT-LLM (NVIDIA, 2023) partially remedy this issue by batching multiple decoding requests, improving the computational intensity of the linear layers. However, the batch size is limited by the memory capacity as each sequence in a batch requires its own KV cache. Furthermore, the computational intensity of the attention operation during decoding is unaffected by batch size, instead requiring a GEMV for each sequence. Grouped query attention (GQA) (Ainslie et al., 2023) converts the operation into a thin GEMM, but it remains memory-bound. This slowdown becomes more evident at longer sequence lengths, where the attention FLOPs continue to increase in proportion to sequence length while the FLOPs required for linear layers remain constant.

### 5.2. Calculating inference FLOPs

While previous works (Patel et al., 2024) have evaluated inference performance using time to first token (TTFT) and time per output token (TPOT), these metrics do not facilitate comparisons across different inference stages, model sizes, or sequence lengths. To ensure a consistent comparison, we directly compute model FLOPs. Following the approach of Ansel et al. (2024); Narayanan et al. (2021), we calculate only the FLOPs associated with matrix multiplication, as these dominate LLM computations. However, unlike previous works, we exclude FLOPs related to autoregressive attention masking, which can be skipped (Dao, 2024). This approach aligns more closely with how the KV cache is leveraged when generating new tokens.

Using this method, the FLOPs required for a forward pass of a Llama model with  $l$  transformer blocks, hidden size  $h$ , intermediate size  $ah$ , head size  $d$ , head count  $H = h/d$ , GQA group size  $g$ , vocabulary size  $v$ , and input sequence of length  $s$  can be calculated as follows:

$$f_{llama}(s) = 2sh^2l(3a + 2 + \frac{2}{g}) + 2s^2hl + 2vsh \quad (2)$$

By denoting  $A = (3a + 2 + \frac{2}{g})$  as a constant for each model, the equation can be simplified to the following:

$$f_{llama}(s) = 2s(Ah^2l + vh) + 2s^2hl \quad (3)$$

When the model generates  $t$  tokens in a single decoding iteration where  $t \ll s$ , we can calculate Equation 2 using  $s' = s + t$  and obtain the approximation:

$$\begin{aligned} & f_{llama}(s + t) - f_{llama}(s) \\ & \approx 2t(Ah^2l + vh) + 4sth \end{aligned} \quad (4)$$

From Equation 4, we observe that linear layer computations,

including those in the LM head, remain independent of the previous sequence length  $s$ . However, attention computations scale proportionally with  $s$ . In the autoregressive case where  $t = 1$  and considering a batch of sequences with batch size  $b$  and sequence lengths  $s_1, \dots, s_b$ , the FLOPs per decoding step can be approximated as follows:

$$2b(Ah^2l + vh) + 4hl \sum_{i=1}^b s_i \quad (5)$$

One challenge in interpreting these results is that only the  $2bAh^2l$  term, representing linear layers except the LM head, is computed in FP8, whereas the  $2bvh$  term for the LM head and the  $4hl \sum_{i=1}^b s_i$  term for attention are computed in BF16. Another is that online KV cache dequantization would add non-trivial overhead to Equation 5. However, such overheads do not constitute additional model FLOPs as per the definition of MFU in Chowdhery et al. (2023).

A more significant limitation is that each FLOP cannot be executed at full efficiency due to hardware utilization constraints. For example, the Gaudi 2 has a peak HBM bandwidth of 2.4 TB/s and a peak FP8 GEMM throughput of 865 TFLOPS, requiring a FLOP/byte ratio (computational intensity, CI) of at least 360 for optimal FP8 execution. However, in the decoding phase, a thin GEMM of  $(b \times h) \times (h \times ah)$ , where  $b \ll h$  and  $a \geq 1$ , results in a CI of approximately  $2b$  for FP8 and  $b$  for BF16, far below the required intensity for peak throughput on realistic batch sizes  $b$ . Additionally, matrix multiplication units operate with fixed block sizes, meaning that full utilization is only achieved when input dimensions align with hardware-friendly shapes such as multiples of 128 (Lee et al., 2024).

Furthermore, KV cache computations present a unique bottleneck. Increasing batch size does not improve the CI since each sequence in a batch maintains a separate KV cache. For a BF16 KV cache using GQA with  $g$  groups, the CI is thus limited to  $g$  FLOPs/byte. Consequently, even with a perfectly optimized kernel, the theoretical throughput of applying the query to the KV cache is capped by the memory bandwidth multiplied by the CI. For Llama v3 models with  $g = 8$  on a Gaudi 2 with a peak 2.4 TB/s HBM, this theoretical ceiling is 19.2 TFLOPS, a small fraction of peak GEMM throughput. As attention computations are both inherently memory-bound and scale linearly with sequence length, decoding at longer sequence lengths ultimately converges to the attention throughput, as demonstrated in Figure 1.

By distinguishing these phases and understanding their computational characteristics, optimization strategies can be tailored to enhance the efficiency of LLM inference, especially during the resource-intensive decode phase.

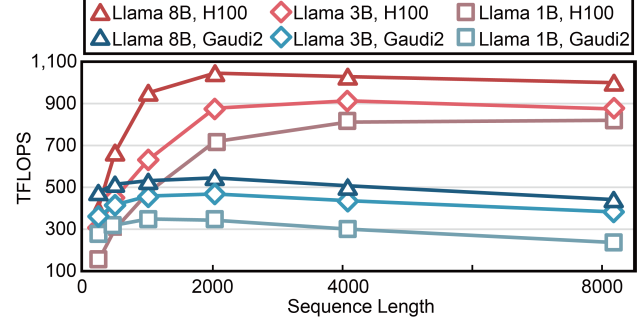


Figure 3. Roofline diagram during the prefill phase for batch size 1. Throughput improves with longer sequence length until it begins to decline as the proportion of attention computations, which are slower than GEMMs, take up a greater share of the computation. We use static FP8 scaling for both the H100 and the Gaudi 2 as optimized dynamic FP8 scaling is unavailable for the Gaudi.

### 5.3. Prefill phase

We first conducted an analysis of the operational characteristics of the two accelerators in the prefill phase. Figure 3 compares the prefill TFLOPS achieved for three models across varying sequence lengths, using a roofline diagram for the H100 and Gaudi 2 accelerators. The results demonstrate that the H100 achieves significantly higher throughput during the prefill phase than the Gaudi 2. For Llama 8B, the H100 achieves double the throughput of the Gaudi 2.

During the prefill phase, attention layers process long input sequences, enabling large matrix computations to be executed in a single step. This maximizes compute engine utilization, leading to high efficiency. As a result, performance in this phase is primarily dictated by GEMM throughput, rather than utilization or memory bandwidth constraints.

As model sizes increase, matrix dimensions grow proportionally with hidden dimensions, making computations more compute-bound. This leads to a clear trend of increasing prefill throughput with larger models, underscoring the importance of compute performance in the prefill phase. A similar pattern is observed for longer sequence lengths, where utilization improves until reaching saturation.

### 5.4. Decode phase

In Figure 1, we compare decode throughputs between the Gaudi 2 and H100. Surprisingly, the Gaudi 2 not only demonstrates superior power efficiency across all sequence lengths but also achieves higher absolute throughput for short sequences below 4K tokens. At longer sequence lengths, however, memory bandwidth becomes the primary bottleneck. Our measurements show HBM bandwidths of 2.0 TB/s for the Gaudi 2 and 2.6 TB/s for the H100, giving the latter an advantage as the KV cache size increases.

We also compare decode throughputs for BF16, dynamic

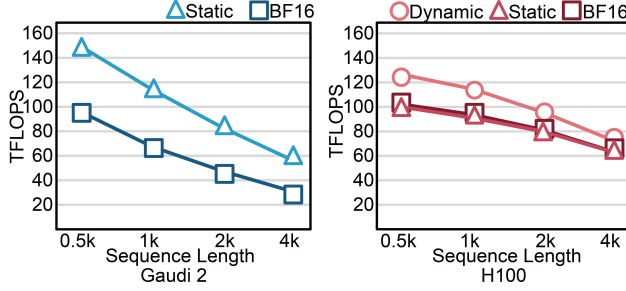


Figure 4. Decode throughput comparison between BF16 and FP8 on Llama v3.1 8B Instruct using a batch size of 64 using static FP8 scaling on the Gaudi 2 (left); static and dynamic FP8 scaling on the H100 (right). Throughput differences between FP8 and BF16 in the Gaudi 2 are 50% or greater, whereas they are under 25% for the H100. Dynamic scaling has higher throughput despite its greater overhead because row-wise GEMM is faster than per-tensor GEMM for small matrices on the H100 (see Table 9).

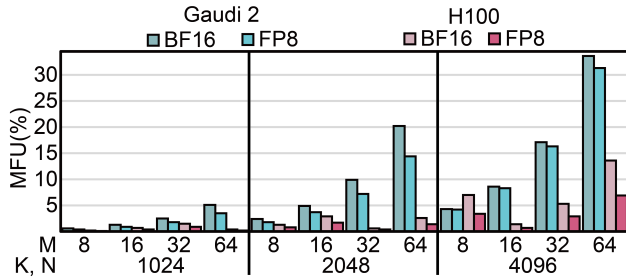


Figure 5. Thin GEMM MFU comparison between the Gaudi 2 and H100 for both BF16 and FP8. The Gaudi 2 maintains similar MFU for BF16 and FP8 for similar shapes while there is a noticeable drop for the H100. The MFU differences at the same shapes are enough to provide superior TFLOPS for the Gaudi 2 over the H100 as shown in Table 4.

FP8 scaling, and static FP8 scaling on the H100 in Figure 4 and find that the throughput gain from FP8 is below 25%. In contrast, the gain for the Gaudi 2 approaches 50%.

To investigate the lack of performance gains in the H100, we analyze its throughput on thin matrices, identifying it as the primary bottleneck. Table 4 shows that while FP8 GEMM throughput on the Gaudi 2 is nearly twice that of BF16 GEMM, there is minimal improvement on the H100. As shown in Equation 5, the decoding stage at short sequence lengths ( $s < h$ ) is dominated by linear operations, making thin GEMM performance critical.

## 6. Conclusion

In this study, we provide a comprehensive analysis of FP8, an emerging numerical format that remains underexplored. We examine various FP8 scaling factor configurations and analyze LLM inference workloads based on the constraints of real-world data center environments. We make a clear exposition of the key constraints in LLM inference, also

Table 4. Thin GEMM throughputs in TFLOPS for the Gaudi 2 and H100 measuring  $(M \times K) \times (K \times N)$  GEMMs, where  $M$  corresponds to typical batch sizes encountered during inference and  $K, N$  represent hidden dimension sizes. Row-wise scaling is used for FP8 GEMMs. Throughput scales linearly with  $M$  on both devices, but the Gaudi 2 consistently outperforms the H100, even for BF16. These results highlight the superior efficiency of the Gaudi 2 for thin GEMMs, crucial for LLM decoding.

GEMM TFLOPS Shape: (M,K,N)	Gaudi 2		H100	
	BF16	FP8	BF16	FP8
(8, 1024, 1024)	3.3	3.8	1.7	1.7
(16, 1024, 1024)	6.5	11.4	3.4	3.9
(32, 1024, 1024)	12.8	23.8	6.5	7.0
(64, 1024, 1024)	26.7	54.0	12.6	14.9
(8, 2048, 2048)	12.4	26.1	6.7	7.5
(16, 2048, 2048)	20.6	48.6	12.9	15.0
(32, 2048, 2048)	48.0	87.6	27.1	28.2
(64, 2048, 2048)	91.3	163.2	52.3	60.5
(8, 4096, 4096)	18.8	35.4	14.4	16.8
(16, 4096, 4096)	37.4	67.9	28.6	33.5
(32, 4096, 4096)	73.6	132.0	68.3	68.1
(64, 4096, 4096)	144.5	253.4	133.3	133.9

providing a framework to make precise calculations for inference throughput. Our analysis of the two phases of LLM inference highlights the strong dependence of LLM inference on hardware characteristics.

However, beyond hardware development, software optimizations that fully leverage accelerator capabilities are equally essential to maximizing performance. One key limitation of the Gaudi is its limited software support and integration. For instance, many kernel fusion techniques for dynamic FP8 scaling are currently unavailable on the Gaudi. Additionally, the decode throughputs reported in our study relied on static memory allocation as the paged attention implementations remained uncompetitive despite recent optimizations (Lee et al., 2024). Even for static memory allocation, the observed attention throughputs are lower than what would be expected from the hardware specifications. Furthermore, while not a primary focus of this work, the lack of KV cache quantization support present challenges for deployment.

Despite these concerns, the growing adoption of inference-time scaling via chain-of-thought (CoT) (Wei et al., 2022) prompting suggests that LLM workloads will increasingly be dominated by decoding. Emerging techniques that decouple the prefill and decode phases (Patel et al., 2024; Zhong et al., 2024) enable hardware to be allocated to the tasks for which they are best suited. Given our findings that the Gaudi 2 demonstrates superior decoding efficiency for FP8, this has potential implications for cloud service providers seeking cost-effective inference solutions.

## References

Ainslie, J., Lee-Thorp, J., de Jong, M., Zemlyanskiy, Y., Lebron, F., and Sanghai, S. GQA: Training generalized multi-query transformer models from multi-head checkpoints. In *The 2023 Conference on Empirical Methods in Natural Language Processing*, 2023. URL <https://openreview.net/forum?id=hm0wOZWzYE>.

Ansel, J., Yang, E., He, H., Gimelshein, N., Jain, A., Voznesensky, M., Bao, B., Bell, P., Berard, D., Burovski, E., Chauhan, G., Chourdia, A., Constable, W., Desmaison, A., DeVito, Z., Ellison, E., Feng, W., Gong, J., Gschwind, M., Hirsh, B., Huang, S., Kalambarkar, K., Kirsch, L., Lazos, M., Lezcano, M., Liang, Y., Liang, J., Lu, Y., Luk, C. K., Maher, B., Pan, Y., Puhrsch, C., Reso, M., Saroufim, M., Siraichi, M. Y., Suk, H., Zhang, S., Suo, M., Tillet, P., Zhao, X., Wang, E., Zhou, K., Zou, R., Wang, X., Mathews, A., Wen, W., Chanan, G., Wu, P., and Chintala, S. Pytorch 2: Faster machine learning through dynamic python bytecode transformation and graph compilation. In *Proceedings of the 29th ACM International Conference on Architectural Support for Programming Languages and Operating Systems, Volume 2*, ASPLOS '24, pp. 929–947, New York, NY, USA, 2024. Association for Computing Machinery. ISBN 9798400703850. doi: 10.1145/3620665.3640366. URL <https://doi.org/10.1145/3620665.3640366>.

Ashkboos, S., Mohtashami, A., Croci, M. L., Li, B., Cameron, P., Jaggi, M., Alistarh, D., Hoefer, T., and Hensman, J. Quarot: Outlier-free 4-bit inference in rotated LLMs. In *The Thirty-eighth Annual Conference on Neural Information Processing Systems*, 2024. URL <https://openreview.net/forum?id=dfqsW38v1X>.

Chowdhery, A., Narang, S., Devlin, J., Bosma, M., Mishra, G., Roberts, A., Barham, P., Chung, H. W., Sutton, C., Gehrmann, S., Schuh, P., Shi, K., Tsvyashchenko, S., Maynez, J., Rao, A., Barnes, P., Tay, Y., Shazeer, N., Prabhakaran, V., Reif, E., Du, N., Hutchinson, B., Pope, R., Bradbury, J., Austin, J., Isard, M., Gur-Ari, G., Yin, P., Duke, T., Levskaia, A., Ghemawat, S., Dev, S., Michalewski, H., Garcia, X., Misra, V., Robinson, K., Fedus, L., Zhou, D., Ippolito, D., Luan, D., Lim, H., Zoph, B., Spiridonov, A., Sepassi, R., Dohan, D., Agrawal, S., Omernick, M., Dai, A. M., Pillai, T. S., Pelлат, M., Lewkowycz, A., Moreira, E., Child, R., Polozov, O., Lee, K., Zhou, Z., Wang, X., Saeta, B., Diaz, M., Firat, O., Catasta, M., Wei, J., Meier-Hellstern, K., Eck, D., Dean, J., Petrov, S., and Fiedel, N. Palm: scaling language modeling with pathways. *J. Mach. Learn. Res.*, 24(1), January 2023. ISSN 1532-4435.

Dao, T. Flashattention-2: Faster attention with better parallelism and work partitioning. In *The Twelfth International Conference on Learning Representations*, 2024. URL <https://openreview.net/forum?id=mZn2Xyh9Ec>.

DeepSeek-AI. Deepseek-v3 technical report, 2024. URL <https://arxiv.org/abs/2412.19437>.

DeepSeek-AI. Deepseek-r1: Incentivizing reasoning capability in llms via reinforcement learning, 2025. URL <https://arxiv.org/abs/2501.12948>.

Ding, N., Chen, Y., Xu, B., Qin, Y., Hu, S., Liu, Z., Sun, M., and Zhou, B. Enhancing chat language models by scaling high-quality instructional conversations. In Bouamor, H., Pino, J., and Bali, K. (eds.), *Proceedings of the 2023 Conference on Empirical Methods in Natural Language Processing*, pp. 3029–3051, Singapore, December 2023. Association for Computational Linguistics. doi: 10.18653/v1/2023.emnlp-main.183. URL <https://aclanthology.org/2023.emnlp-main.183>.

El Arar, E.-M., Sohier, D., de Oliveira Castro, P., and Petit, E. Stochastic rounding variance and probabilistic bounds: A new approach. *SIAM Journal on Scientific Computing*, 45(5):C255–C275, 2023. doi: 10.1137/22M1510819. URL <https://doi.org/10.1137/22M1510819>.

Fan, H., Zhou, H., Huang, G., Raman, P., Fu, X., Gupta, G., Ram, D., Wang, Y., and Huan, J. HLAT: High-quality Large Language Model Pre-trained on AWS Trainium. In *2024 IEEE International Conference on Big Data (BigData)*, pp. 2100–2109, Los Alamitos, CA, USA, December 2024. IEEE Computer Society. doi: 10.1109/BigData62323.2024.10825098. URL <https://doi.ieee.org/10.1109/BigData62323.2024.10825098>.

Frantar, E. and Alistarh, D. Sparsegpt: massive language models can be accurately pruned in one-shot. In *Proceedings of the 40th International Conference on Machine Learning*, ICML'23. JMLR.org, 2023.

Frantar, E., Ashkboos, S., Hoefer, T., and Alistarh, D. OPTQ: Accurate quantization for generative pre-trained transformers. In *The Eleventh International Conference on Learning Representations*, 2023. URL <https://openreview.net/forum?id=tcbBPnfwxS>.

Frantar, E., Castro, R. L., Chen, J., Hoefer, T., and Alistarh, D. Marlin: Mixed-precision auto-regressive parallel inference on large language models. *arXiv preprint arXiv:2408.11743*, 2024.

Gao, L., Tow, J., Abbasi, B., Biderman, S., Black, S., DiPofi, A., Foster, C., Golding, L., Hsu, J., Le Noac'h, A., Li, H., McDonell, K., Muennighoff, N., Ociepa, C., Phang, J., Reynolds, L., Schoelkopf, H., Skowron, A., Sutawika, L., Tang, E., Thite, A., Wang, B., Wang, K., and Zou, A. A framework for few-shot language model evaluation, 07 2024. URL <https://zenodo.org/records/12608602>.

Hendrycks, D., Burns, C., Basart, S., Zou, A., Mazeika, M., Song, D., and Steinhardt, J. Measuring massive multitask language understanding. In *International Conference on Learning Representations*, 2021. URL <https://openreview.net/forum?id=d7KBjmI3GmQ>.

Intel. Intel gaudi 2 ai accelerator white paper, 2022. URL <https://cdrv2-public.intel.com/784827/Gaudi2%20White%20Paper.pdf>. Accessed: 2025-01-31.

Intel. Intel gaudi 3 ai accelerator white paper, 2024. URL <https://cdrv2-public.intel.com/817486/gaudi-3-ai-accelerator-white-paper.pdf>. Accessed: 2025-01-31.

Kalamkar, D., Mudigere, D., Mellempudi, N., Das, D., Banerjee, K., Avancha, S., Vooturi, D. T., Jammalamadaka, N., Huang, J., Yuen, H., Yang, J., Park, J., Heinecke, A., Georganas, E., Srinivasan, S., Kundu, A., Smelyanskiy, M., Kaul, B., and Dubey, P. A study of bfloat16 for deep learning training, 2019. URL <https://arxiv.org/abs/1905.12322>.

Kim, M. [intel gaudi] #4. fp8 quantization, 2025. URL <https://blog.squeezebits.com/intel-gaudi-4-fp8-quantization--40269>.

Kurtic, E., Marques, A., Pandit, S., Kurtz, M., and Alistarh, D. "give me bf16 or give me death"? accuracy-performance trade-offs in llm quantization, 2024. URL <https://arxiv.org/abs/2411.02355>.

Kwon, W., Li, Z., Zhuang, S., Sheng, Y., Zheng, L., Yu, C. H., Gonzalez, J. E., Zhang, H., and Stoica, I. Efficient memory management for large language model serving with pagedattention. In *Proceedings of the ACM SIGOPS 29th Symposium on Operating Systems Principles*, 2023.

Lee, J. H., Kim, J., Kwon, S. J., and Lee, D. Flexround: learnable rounding based on element-wise division for post-training quantization. In *Proceedings of the 40th International Conference on Machine Learning*, ICML'23. JMLR.org, 2023.

Lee, Y., Lim, J., Bang, J., Cho, E., Jeong, H., Kim, T., Kim, H., Lee, J., Im, J., Hwang, R., Kwon, S. J., Lee, D., and Rhu, M. Debunking the cuda myth towards gpu-based ai systems, 2024. URL <https://arxiv.org/abs/2501.00210>.

Lin, J., Tang, J., Tang, H., Yang, S., Chen, W.-M., Wang, W.-C., Xiao, G., Dang, X., Gan, C., and Han, S. Awq: Activation-aware weight quantization for on-device llm compression and acceleration. In Gibbons, P., Pekhimenko, G., and Sa, C. D. (eds.), *Proceedings of Machine Learning and Systems*, volume 6, pp. 87–100, 2024a.

Lin, Y., Tang, H., Yang, S., Zhang, Z., Xiao, G., Gan, C., and Han, S. Qserve: W4a8kv4 quantization and system co-design for efficient llm serving. *arXiv preprint arXiv:2405.04532*, 2024b.

Liu, Z., Zhao, C., Fedorov, I., Soran, B., Choudhary, D., Krishnamoorthi, R., Chandra, V., Tian, Y., and Blankevoort, T. Spinquant–llm quantization with learned rotations. *arXiv preprint arXiv:2405.16406*, 2024.

Llama Team, A. . M. The llama 3 herd of models, 2024. URL <https://arxiv.org/abs/2407.21783>.

Merity, S., Xiong, C., Bradbury, J., and Socher, R. Pointer sentinel mixture models. In *International Conference on Learning Representations*, 2017. URL <https://openreview.net/forum?id=Byj72udxe>.

Micikevicius, P., Stosic, D., Burgess, N., Cornea, M., Dubey, P., Grisenthwaite, R., Ha, S., Heinecke, A., Judd, P., Kamalu, J., Mellempudi, N., Oberman, S., Shoeybi, M., Siu, M., and Wu, H. Fp8 formats for deep learning, 2022. URL <https://arxiv.org/abs/2209.05433>.

Narayanan, D., Shoeybi, M., Casper, J., LeGresley, P., Patwary, M., Korthikanti, V., Vainbrand, D., Kashinkunti, P., Bernauer, J., Catanzaro, B., Phanishayee, A., and Zaharia, M. Efficient large-scale language model training on gpu clusters using megatron-lm. In *Proceedings of the International Conference for High Performance Computing, Networking, Storage and Analysis*, SC '21, New York, NY, USA, 2021. Association for Computing Machinery. ISBN 9781450384421. doi: 10.1145/3458817.3476209. URL <https://doi.org/10.1145/3458817.3476209>.

Noune, B., Jones, P., Justus, D., Masters, D., and Luschi, C. 8-bit numerical formats for deep neural networks, 2022. URL <https://arxiv.org/abs/2206.02915>.

NVIDIA. Tensorrt-llm, 2023. URL <https://github.com/NVIDIA/TensorRT-LLM>.

Patel, P., Choukse, E., Zhang, C., Shah, A., Goiri, I., Maleki, S., and Bianchini, R. Splitwise: Efficient generative llm inference using phase splitting. In *2024 ACM/IEEE 51st Annual International Symposium on*

*Computer Architecture (ISCA)*, pp. 118–132, 2024. doi: 10.1109/ISCA59077.2024.00019.

Shazeer, N. Glu variants improve transformer, 2020. URL <https://arxiv.org/abs/2002.05202>.

Shen, H., Mellempudi, N., He, X., Gao, Q., Wang, C., and Wang, M. Efficient post-training quantization with fp8 formats. In Gibbons, P., Pekhimenko, G., and Sa, C. D. (eds.), *Proceedings of Machine Learning and Systems*, volume 6, pp. 483–498, 2024.

Sun, M., Chen, X., Kolter, J. Z., and Liu, Z. Massive activations in large language models. *arXiv preprint arXiv:2402.17762*, 2024a.

Sun, M., Liu, Z., Bair, A., and Kolter, J. Z. A simple and effective pruning approach for large language models. In *The Twelfth International Conference on Learning Representations*, 2024b. URL <https://openreview.net/forum?id=PxoFut3dWW>.

Wei, J., Wang, X., Schuurmans, D., Bosma, M., Ichter, B., Xia, F., Chi, E. H., Le, Q. V., and Zhou, D. Chain-of-thought prompting elicits reasoning in large language models. In *Proceedings of the 36th International Conference on Neural Information Processing Systems*, NIPS '22, Red Hook, NY, USA, 2022. Curran Associates Inc. ISBN 9781713871088.

Wilkinson, L. Introducing machete, a mixed-input gemm kernel optimized for nvidia hopper gpus, 2024.

Xiao, G., Lin, J., Seznec, M., Wu, H., Demouth, J., and Han, S. Smoothquant: Accurate and efficient post-training quantization for large language models, 2024. URL <https://arxiv.org/abs/2211.10438>.

Xiong, R., Yang, Y., He, D., Zheng, K., Zheng, S., Xing, C., Zhang, H., Lan, Y., Wang, L., and Liu, T.-Y. On layer normalization in the transformer architecture. In *Proceedings of the 37th International Conference on Machine Learning*, ICML'20. JMLR.org, 2020.

Zhong, Y., Liu, S., Chen, J., Hu, J., Zhu, Y., Liu, X., Jin, X., and Zhang, H. Distserve: Disaggregating prefill and decoding for goodput-optimized large language model serving. In *OSDI*, pp. 193–210, 2024. URL <https://www.usenix.org/conference/osdi24/presentation/zhong-yinmin>.

## A. Appendix

Table 5. MMLU result for per-row, per-tensor options

model	Rowwise Scaling		accuracy
	Activation	Weight	
Llama-3.2-1B	✓	✓	35.12%
	✓	✓	34.69%
		✓	34.36%
			34.65%
Llama-3.2-3B	✓	✓	53.90%
	✓	✓	53.92%
		✓	53.83%
			53.75%
Llama-3.1-8B	✓	✓	62.95%
	✓	✓	62.92%
		✓	62.80%
			62.90%
Llama-3.1-70B	✓	✓	75.25%
	✓	✓	75.23%
		✓	75.32%
			75.39%

Table 6. MMLU 5-shot CoT for stochastic rounding using E4M3.

Model	Stochastic Rounding		MMLU accuracy
	Activation	Weight	
Llama-3.2-1B	✓	✓	33.94%
	✓	✓	34.31%
		✓	35.20%
			34.65%
Llama-3.2-3B	✓	✓	54.09%
	✓	✓	53.95%
		✓	54.41%
			53.75%
Llama-3.1-8B	✓	✓	62.24%
	✓	✓	62.43%
		✓	62.55%
			62.90%
Llama-3.1-70B	✓	✓	75.05%
	✓	✓	75.18%
		✓	75.30%
			75.39%

Table 7. Throughput and Power Measurement of Llama Instruct Models

Model Name	Mode	Batch Size	Seq Len	Power(W)	Prefill TFLOPS/HPU
Llama-3.2-1B-Instruct	FP8-Static	4	512	509	412
Llama-3.2-1B-Instruct	FP8-Static	4	1024	509	411
Llama-3.2-3B-Instruct	FP8-Static	4	512	498	518
Llama-3.2-3B-Instruct	FP8-Static	4	1024	511	537
Llama-3.1-8B-Instruct	FP8-Static	4	512	471	588
Llama-3.1-8B-Instruct	FP8-Static	4	1024	436	595

Table 8. Gaudi 2 throughput in TFLOPS for scaled FP8 GEMM for square matrices of the given size, excluding quantization overhead. Measured throughput relative to the peak FP8 throughput (865 TFLOPS) is included in parentheses. Hardware acceleration is only available for per-tensor scaling.

Type	Size	Per-Row	Per-Tensor	HW Accel.
E4M3	1K	494 (57.1%)	494 (57.1%)	494 (57.1%)
	2K	506 (58.5%)	641 (74.1%)	641 (74.2%)
	4K	735 (84.9%)	796 (92.1%)	801 (92.6%)
	8K	742 (85.7%)	822 (95.0%)	852 (98.4%)
E5M2	1K	306 (35.4%)	494 (57.1%)	493 (57.0%)
	2K	506 (58.5%)	642 (74.2%)	642 (74.2%)
	4K	735 (84.9%)	802 (92.7%)	802 (92.7%)
	8K	726 (83.9%)	825 (95.4%)	825 (95.4%)

Table 9. H100 throughput in TFLOPS for scaled FP8 GEMM for square matrices of the given size, excluding quantization overhead. Measured throughput as a ratio of peak FP8 throughput (1989.9 TFLOPS) is included in parentheses. We only include results for E4M3 because we were unable to find libraries exposing low-level E5M2 GEMM APIs on NVIDIA GPUs.

Accum.	Size	Per-Row	Per-Tensor
FP32	1K	217 (11.0%)	186 (9.4%)
	2K	299 (15.1%)	840 (42.4%)
	4K	362 (18.3%)	1099 (55.5%)
	8K	396 (20.0%)	1300 (65.7%)
Fast	1K	237 (12.0%)	147 (7.4%)
	2K	810 (40.9%)	896 (45.3%)
	4K	1136 (57.4%)	1205 (60.9%)
	8K	1123 (56.8%)	1388 (70.1%)